Thermoelectric Fibers

Ting Zhang, Haisheng Chen, and Xinghua Zheng

Abstract Flexible thermoelectrics enables a direct and green conversion between heat and electricity to power or refrigerate flexible and wearable electronics. Organic polymer-based flexible thermoelectric materials are particularly fascinating because of their intrinsic flexibility, affordability, and low toxicity, but low thermoelectric performance limits their development. The other promising alternatives of inorganic-based flexible thermoelectric materials that have high energy-conversion efficiency, large power output, and stability at relatively high temperature, yet it is impeded by inferior flexibility. Hence, researchers propose a paradigm shift in material research as flexible thermoelectrics requires the material of which the device is made to simultaneously have inorganic semiconductor-like high thermoelectric performance and organic material-like mechanical flexibility. In this chapter, this dilemma is tackled, on both material level and device level, by introducing a new kind of flexible thermoelectric fibers, which overcomes the problems that thin film-based thermoelectrics can only be bent in one direction and lack essential wearable properties such as air permeability. Herein, the state-of-the-art in the development of flexible thermoelectric fibers and devices is summarized, including organic conducting polymer thermoelectric fibers, fully inorganic flexible thermoelectric fibers, and inorganic TE materials hybridized with organic polymer fibers. Finally, the remaining challenges in flexible thermoelectric fibers are discussed in conclusion, and suggestions and a framework to guide future development are provided, which may pave the way for a bright future of fiber-based flexible thermoelectric devices in the energy market.

Keywords Thermoelectric (TE) fibers · Wearable electronics · Seebeck coefficient · Thermal conductivity · Electrical conductivity · Power factor · ZT

T. Zhang (✉) · H. Chen · X. Zheng
Institute of Engineering Thermophysics, Chinese Academy of Sciences,
Beijing 100190, China
e-mail: zhangting@iet.cn

H. Chen
e-mail: chen_hs@iet.cn

X. Zheng
e-mail: zhengxh@iet.cn

value · PEDOT: PSS fiber · Thermal drawing · Wet-spinning · Electrospun ·
Mechanical flexibility · Conductive polymers · Power output

1 Introduction

In fossil fuel combustion, typically only $\sim 34\%$ of the resulting energy is used effi-
ciently, while the remainder is lost to the environment as waste heat (Fitriani et al.
2016). Broad societal needs have focused attention on technologies that can reduce
ozone depletion, greenhouse gas emissions, and fossil fuel usage. Thermoelectric
(TE) devices, which are semiconductor systems that can directly convert between
thermal and electrical energy, are increasingly being seen as having the potential
to make important contributions to reducing CO_2 and greenhouse gas emissions
and providing cleaner forms of energy. TE devices exhibit many advantages, such
as having no moving parts, no moving fluids, no noise, easy (or no) maintenance,
and high reliability, which has been commercially used for a variety of applica-
tions, including thermal cycles for DNA synthesizers, car seat cooler/heaters, laser
diode coolers, certain low-wattage power generators, and radioisotope thermoelectric
generators, etc. (Du et al. 2018).

TE materials offer a way to convert low-grade waste heat energy into electrical
power, based on the Seebeck effect (Fig. 1a) (Du et al. 2018). This effect was discov-
ered in 1821 by German scientist Thomas Johann Seebeck and can be used in a
wide range of energy-conversion applications. The TE energy-harvesting mecha-
nism of a material is that when a temperature gradient (ΔT) is applied, the charge
carriers (electrons for n-type materials or holes for p-type materials) from the hot
side diffuse to the cold side. As a result, an electrostatic potential (ΔV) is induced
(Li et al. 2010). The electrostatic potential generated by a single n- or p-type TE legs
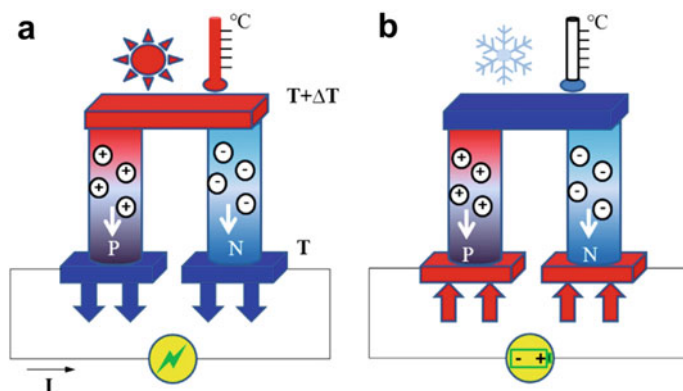is very low (from several μV to mV depending on context). Therefore, to achieve

Fig. 1 Schematic illustrations of a TE module for **a** power generation (Seebeck effect) and **b** active
refrigeration (Peltier effect). Reproduced with permission. (Du et al. 2018) Copyright 2018, Elsevier

high output voltage and power, TE generators are typically made of dozens, or even hundreds, of TE couples. TE materials can also convert electrical power into thermal energy (i.e., cooling or heating) based on the Peltier effect (Fig. 1b) (Du et al. 2018), discovered in 1834 by French scientist Jean Charles Athanase Peltier. The Peltier effect is essentially the inverse of the Seebeck effect. The efficiency of TE devices is strongly associated with the dimensionless figure of merit (ZT) of TE materials, defined as $ZT = (S^2\sigma/\kappa)\,T$, where S, σ, κ and T are the Seebeck coefficient, electrical conductivity, thermal conductivity, and absolute temperature (Du et al. 2018). High electrical conductivity (corresponding to low Joule heating), a large Seebeck coefficient (corresponding to large potential difference) and low thermal conductivity (corresponding to a large temperature difference) are therefore necessary in order to realize high-performance TE materials. The ZT value is also a very convenient indictor for evaluating the potential efficiency of TE devices. In general, good TE materials have a ZT value of close to unity. However, ZT values of up to three are considered to be essential for TE energy converters that can compete on efficiency with mechanical power generation and active refrigeration (Li et al. 2010).

High-performance TE materials have been pursued since Bi_2Te_3-based alloys were discovered in the 1960s. Until the end of last century, moderate progress had been made in the development of TE materials. The benchmark of $ZT \approx 1$ was broken in the mid-1990s by two different research approaches: one by exploring new materials with complex crystalline structures, and the other by reducing the dimensions of the materials (Li et al. 2010). In the recently discovered TE compounds, such as skutterudites, clathrates, and Zintl compounds, the thermal conductivity can be reduced greatly while maintaining the electrical conductivity at a high level (Lan et al. 2010). In research on low-dimensional material systems, Dresselhaus et al. suggested that the power factor ($P = S^2\sigma$) can be enhanced through the use of quantum confinement effects. Dresselhaus's pioneering work has shed light on various low-dimensional systems, including superlattices, nanowires, and quantum dots (Dresselhaus et al. 2007). Venkatasubramanian et al. reported Bi_2Te_3/Sb_2 Te_3 superlattices with a high-ZT value of up to 2.4 (Venkatasubramanian et al. 2001). Subsequently, Harman et al. reported PbTe/PbTeSe quantum dot superlattices with a ZT value of greater than 3.0 at 600 K (Harman et al. 2002). However, these high-ZT low-dimensional materials are difficult to be applied on general applications, and it is still desired to develop potential routes for improvement in the major TE bulk material systems, including Bi–Te alloys, skutterudites, Ag–Pb–Sb–Te or 'LAST', half-Heusler alloys and some high-ZT oxides (Snyder and Toberer 2008). In 2014, an unprecedented ZT value of 2.6 for bulk materials is realized in SnSe single crystals at 923 K (Zhao et al. 2014), and the hole doped SnSe single crystals exhibit ZT > 1.5 at 600–773 K while the highest value of 2.8 at 773 K for electron-doped SnSe single crystals (Chang et al. 2018). These attributes are generally associated with low thermal conductivity. Compared to other high-performance thermoelectrics, SnSe single crystals demonstrate that a high ZT also can be realized in simple layered, anisotropic and anharmonic systems, without nanostructuring.

Nowadays, TE materials chipped into devices are mostly prepared in the form of cube or cuboid blocks from a TE ingot by means of a top-down dicing process. A
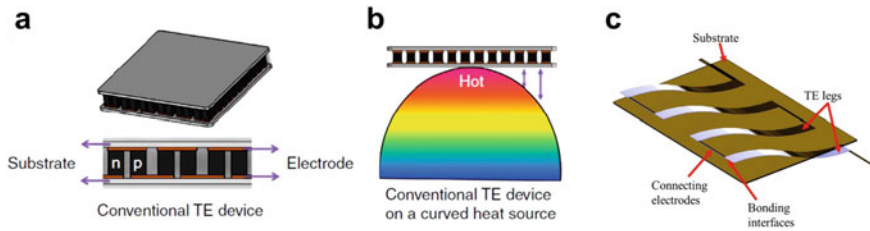
Fig. 2 a A conventional planar-structured TE device. **b** Scheme of power generation of the conventional TE generator on a curved heat source. **c** Schematic diagram of a typical module for flexible TE devices. **a**, **b** Reproduced with permission. (Park et al. 2016) Copyright 2016, Springer Nature. **c** Reproduced with permission. (Wang et al. 2019) Copyright 2019, Wiley-VCH

potential problem of this conventional procedure is a relatively high production cost due to the energy intensive processing for ingots such as zone-melting or hot-pressing as well as the post-processing due to shape control. The latter, in fact, suffers from another problem that attempts to realize any complicated shape other than a cube are technically impossible within the context of mass production. On the other hand, in the real-world applications, the minimization of heat loss due to incomplete contact between the surface of the heat source and the TE module is no less important than the figure-of-merit of materials. It is noted that the majority of heat sources for TE generators has irregular shapes, where the conventional planar-structured TE devices composed of cubic blocks should fail in achieving a desirable contact (Fig. 2a, b) (Park et al. 2016). One readily available solution to settling down the aforementioned issues is the development of flexible TE materials and devices.

Flexible TE materials, in this situation, are promising because their conformability enables effective contact with curved heat sources in order to maximize heat harvesting. These flexible TE materials can also be fabricated at much lower temperatures. Compared with other rigid devices, flexible TE devices are lightweight and can be conformably attached onto human skin, enabling the direct harvesting of electricity from body heat without recharging, but also preventing or minimizing heat losses during energy transfer. Such advantages make flexible TE devices promising power sources for wearable electronics. Figure 1c illustrates a typical flexible TE device, composed of a substrate, TE legs, connecting electrodes, and bonding interfaces (Wang et al. 2019). In such an flexible TE device, the substrates are flexible and insulating in order to provide the devices with flexibility, which guarantees interference-free carrier transport within the TE legs; the TE legs are in the form of thin films, which can be adapted for device flexibility; the electrodes are applied to connect n- and p-type TE legs in series; and the bonding interfaces stabilize the TE legs and electrodes (Chen et al. 2015). Moreover, the Seebeck effect is the primary enabling physical phenomenon that facilities the function of flexible TE devices as potential body temperature monitors by transferring body temperature changes into an output voltage signal (Yang et al. 2018). By the Peltier effect, flexible TE devices can also be applied in flexible temperature-control systems, which can be used in microclimate systems that maintain the body temperature in extreme conditions

(Zhang et al. 2018), medical devices such as cooling blankets (Delkumburewatte and Dias 2012), and emerging portable electronic devices that require cooling (He et al. 2015). Although their applications as power implantable devices are still controversial, with concerns about their toxicity, there is clearly a bright future of flexible TEs.

For flexible TE materials, the most common approaches are to use either fully organic TEs or inorganic/organic hybrids. Some conducting polymers exhibit relatively good TE properties, such as poly(3,4-ethylenedioxythiophene):poly(styrenesulfonate) (PEDOT:PSS), polyaniline, polypyrrole, and their derivatives, due to their intrinsic flexibility and conductivity (Wang and Zhang 2019). Additionally, conductive polymers are abundant, nontoxic, or low toxicity, and generally easy to shape and process for industrial applications. The major drawback of conductive polymers is their poor electrical transport properties, which can be improved by doping and secondary doping engineering (Chen et al. 2015). Nevertheless, higher TE performance (in terms of output power and/or efficiency) may be achieved in inorganic/polymer hybrid materials. For example, in inorganic/organic composite materials, the high electrical conductivity and Seebeck coefficient of the inorganic constituent can be integrated with the low thermal conductivity of the polymers, and thus achieve high TE efficiency. More complex approaches to inorganic/organic hybrid materials include incorporating TE fillers into conductive polymers via ex situ (Du et al. 2014) and in situ synthesis (Gao and Chen 2018), or by intercalating organic molecules into inorganic layered structures (Wan et al. 2015). In such organic/inorganic hybrids, inorganic fillers such as inorganic TE particles and carbon-based nanomaterials can provide extra current pathways and in turn induce energy-filtering effects in the flexible polymer matrix, while organic molecules can provide the desired flexibility for the inorganic host (Gao et al. 2017). For inorganic flexible TE thin films, continuous flexibility can be realized through either depositing inorganic TE thin films on flexible substrates using atomic deposition techniques (Yang et al. 2017), or applying carbon nanotube (CNT) scaffolds (Jin et al. 2019) or nanostructure tailoring (Paul et al. 2017) to develop freestanding inorganic flexible TE films. However, limited by the device size, small temperature gradient, and low energy-conversion efficiency of flexible TE materials, the output power of flexible TE film devices is only a few μW to several mW (Kim et al. 2016). Optimization of the design of devices is another key factor to achieving their high performance. For example, devices have been achieved in the form of fiber-based textile structures, which significantly enhances device performance and essentially meets the wearable requirement of air permeability, showing great promise for the development of TE clothes (Du et al. 2017).

Fiber-shaped electronic devices, adopting one-dimensional (1D) structure with small diameters from tens to hundreds of micrometers, have attracted broad interests for wearable electronic fields (Lan et al. 2010). Typically, fiber-shaped electronic devices can be prepared on the basis of coaxial, twisting, and interlacing architectures. These fiber-shaped electronic devices are lightweight and flexible, and they can adapt to various deformations like bending, distortion, and stretching. More importantly, it is feasible to weave the fiber-shaped electronic devices into flexible,

deformable, and breathable textiles that can facilitate practical applications. Hence, quite lots of researchers have devoted themselves to enhancing device performances (Wang et al. 2020). To make full use of the advantages of fiber and textile electronics, stretchable, self-healing, or shape-memory, fiber-shaped electronic devices have been further developed (Lee et al. 1902). More importantly, people have to realize self-powering devices by integrating energy harvesting with energy storage (Zhu et al. 2020). Fiber-based flexible TE energy generators are 3D deformable, lightweight, and desirable for applications in large-area waste heat recovery, and as energy suppliers for wearable or mobile electronic systems in which large mechanical deformations, high energy-conversion efficiency, and electrical stability are greatly demanded. TE fiber devices can be manufactured at low or room temperature under ambient conditions by established industrial processes, offering cost-effective and reliable products in mass quantity, which has inspired the industry like electronic and clothing industry because fiber-shaped TE devices can be woven through the well-developed commercial textile technology.

Here, we provide a critical overview of the progress of fiber-shaped TE materials and devices. We aim to identify the existing benchmarks, point out current problems, and predict future directions for further improvement. This chapter covers the materials fabrication methods, device structures and potential applications of TE fibers. Discussions are presented on the opportunities and challenges of TE fibers in terms of their device structure and applications. Last, we provide our perspectives on future research directions of fiber-shaped TE devices. We hope that this report will encourage researchers to putting more effort to translate the progress made in research laboratories for developing TE fibers into practical applications.

2   Fiber-Shaped TE Materials and Devices

The selection of appropriate materials is extremely important for the design and fabrication of fiber-shaped TE materials and devices. These materials should possess high energy-conversion efficiency with high carrier mobility and appropriate carrier concentration. Meanwhile, these materials should have the expected thermal and mechanical properties, be flexible and eco-friendly, show stable performance, and be easy to fabricate at low or room temperature using low-cost materials. According to constituent materials, TE fibers can be summarized as organic TE fibers, inorganic TE fibers, and organic/inorganic composite TE fibers.

- **Organic TE fibers**

Conductive polymers are organic materials with intrinsically electrical conduction. Alan Heeger, Alan MacDiarmid, and Hideki Shirakawa first discovered conducting polyacetylene in 1970s. They were jointly awarded with the Nobel Prize in 2000 for this discovery. Like traditional polymers, conducing polymers have a low thermal conductivity when compared to inorganic TE materials, which is beneficial for high

ZT. Furthermore, conducting polymers also have good flexibility, low density, low cost and easy synthesis and processing into versatile forms; therefore, much attention has recently been paid to conducting polymers for TE applications. Aqueous PEDOT:PSS dispersions are commercially available. The properties of PEDOT:PSS vary with the product types and its electrical conductivity, as well as TE properties, can be significantly enhanced by adding secondary dopants or compositing with special semiconductors. Besides, PEDOT:PSS possesses excellent stability, flexible mechanical properties, and high transparency, making it a promising candidate for organic TE materials (Yue and Xu 2012). The maximum ZT at room temperature was 0.42, which was measured from the DMSO-doped PEDOT:PSS (Kim et al. 2013). In addition to the doping method, post-treatments, such as adding solvents or dedoping, have been explored. After treatment, although the ZT was only ≈ 0.1, the power factor was as high as 112 μWm^{-1}K^{-2} (Park et al. 2014). Moreover, H_2SO_4 has proven to be the most effective solvent for conductivity enhancement. After treatment with H_2SO_4, the conductivity of PEDOT:PSS increased and reached ~4380 S cm^{-1} (Kim et al. 2014). These studies suggest that H_2SO_4 is a promising candidate to replace the organic solvents commonly used in the coagulation bath of PEDOT:PSS fiber spinning.

Razal et al. (2019) reported a facile one-step method to produce highly conducting PEDOT:PSS fibers that effectively removes the insulating PSS component within seconds, thereby enabling their fabrication in a fast one-step process. The highest electrical conductivity is 3828 S cm^{-1} for a ~15-micron fiber. PEDOT:PSS fibers were fabricated at room temperature using a custom-made bottom-up wet-spinning apparatus (Fig. 3). Typically, the spinning formulation was loaded into a syringe
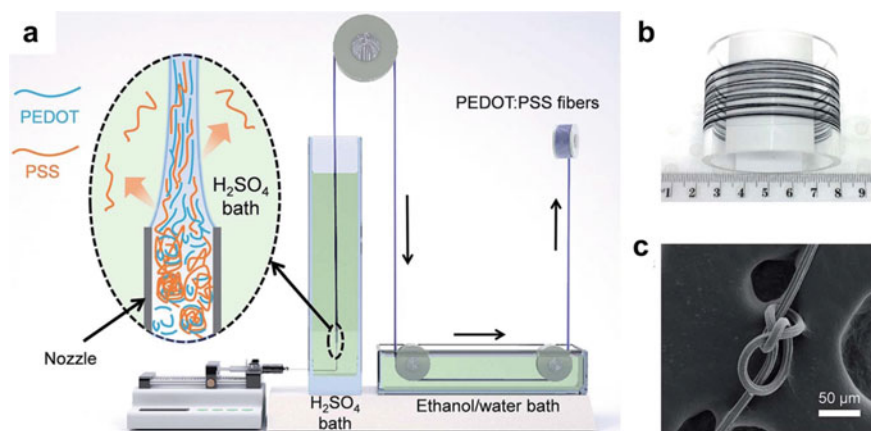

Fig. 3 **a** Schematic illustration of the modified setup used in wet-spinning PEDOT:PSS fibers. Inset shows the schematic illustration of the alignment of PEDOT:PSS domains during fiber formation and the outward diffusion of excess PSS to H_2SO_4 coagulation bath. **b** Sample spool containing over 100 meters of continuous PEDOT:PSS fiber. **c** Representative scanning electron microscopy (SEM) image of a PEDOT:PSS showing great flexibility through tight knots. Reproduced from Ref. (Zhang et al. 2019) with permission from The Royal Society of Chemistry

and then mounted on a syringe pump. The formulation was extruded into H_2SO_4 coagulation bath through a blunt needle from the bottom of the coagulation bath. The fiber was passed through a washing bath of ethanol/water mixture to remove H_2SO_4 from fiber. PEDOT:PSS fibers were dried under tension using a halogen light as heating source and collected by winding onto a spool. Multifilament PEDOT:PSS fibers were produced using the same method by replacing the single needle with a 7-hole spinneret. These fibers can withstand mechanical mistreatment. Testing has been conducted in various environments including sonication and exposure to boiling water for extended periods. The study on the mechanism of conductivity enhancement shows that the spinning method efficiently removes the PSS component during fiber formation and improves orientation of the PEDOT chains, which facilitates efficient intramolecular and intermolecular charge transport, leading to the enhancement in electrical properties.

Xu and his co-workers (Liu et al. 2018) reported that a highly conductive p-type PEDOT:PSS fiber was produced by gelation process, which was three orders of magnitude higher than that of previous hydrogel fibers. In brief, a certain volume of PEDOT:PSS suspension (Clevios, PH1000) containing 0.05 M H_2SO_4 was sealed in a poly(tetrafluoroethylene) capillary (inner diameter = 1.0 mm), which was kept at 90 °C for 3.0 h. To optimize the synthesis procedure, vacuum evaporation was employed to condense the solid content of PEDOT:PSS in solution. After concentration, 5.0 vol.% dimethyl sulfoxide (DMSO) was added into the as-condensed solution following ultrasonic treatment for 10 min. After the formation of hydrogel, the as-obtained fibers were released into isopropyl alcohol (IPA), ethyl alcohol, or acetone bath from capillary by pumping air. They were cleaned by deionized water repeatedly and dried under 60 °C in vacuum for 1.0 h. Then, the resultant fibers were immersed in EG and DMSO (Fig. 4a–c). Finally, the as-prepared fibers were washed with deionized water again for several times and dried at 80 °C for 30 min. Surprisingly, a posttreatment with organic solvents such as EG and DMSO tripled their electrical conductivity with an only 5% decreased Seebeck coefficient, consequently
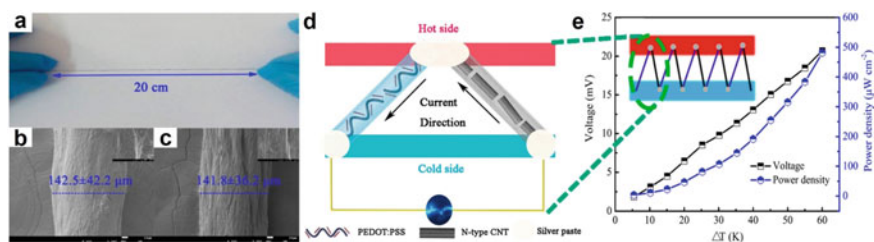

Fig. 4 **a** Digital photographs of as-fabricated PEDOT:PSS fiber. SEM images of PEDOT:PSS fibers **b** before and **c** after ethylene glycol (EG) posttreatment. **d** Schematic diagram for TE device and **e** the output voltage and power density of five couples of legs at various temperature differences ranging from 5 to 60 K. The inset is a scheme for the fiber device consisting of five pairs of p-n legs consisting of EG-treated p-type PEDOT: PSS fibers and n-type CNT fibers. Reproduced with permission. (Liu et al. 2018) Copyright 2017, American Chemical Society

leading to an optimized thermoelectric power factor. Furthermore, they assembled a p-n-type thermoelectric device connecting five pairs of p-type PEDOT:PSS fibers and n-type carbon nanotube fibers (Fig. 4d). This fiber-based device displayed an acceptable output voltage of 20.7 mV and a power density of 481.2 $\mu W \cdot cm^{-2}$ with a temperature difference of $\sim$60 K (Fig. 4e), which might pave the way for the development of organic TE fibers for wearable energy harvesting.

A prerequisite for TE fibers is wash and wear resistance, which is necessary to withstand both textile manufacture and daily use. Integration of the conducting organic material into the fiber, which can be achieved through either incorporation during fiber spinning or impregnation of an existing fiber, is likely to result in a more durable functionalization because a surface coating is prone to delamination during bending and abrasion during wear. The use of natural materials such as polysaccharide-based cotton and protein-based silk offer a number of advantages because they can be derived from renewable sources, are biocompatible, and, being traditional textile materials, are readily compatible with existing manufacturing routines. A lasting wear and wash resistant finish can be realized through functionalization with materials that carry ionizable groups, which is a common feature of acid dyes that are used by the textile industry to color natural fibers such as wool, mohair, and silk. Similarly, water-soluble conjugated polyelectrolytes that carry negatively charged acetate or sulfonate counterions can tightly bind to fiber through electrostatic interactions with cationic sites, provided that the pH is adjusted during the dyeing process to ensure polypeptides with a net positive charge (Müller et al. 2011). Ryan et al. demonstrated that PEDOT:PSS can be used akin to an acid dye. Impregnation of silk from the silkworm Bombyx mori allows realizing durable high-modulus fibers with a bulk electrical conductivity of 14 S cm^{-1} (Fig. 5). A high Young's modulus of approximately 2 GPa combined with a robust and scalable dyeing process results in up to 40 m long fibers that maintain their electrical properties when experiencing repeated bending stress as well as mechanical wear during sewing. Moreover, a high degree of ambient stability is paired with the ability to withstand both machine washing and dry cleaning. To illustrate the potential use for e-textile applications, they realized an in-plane thermoelectric module that comprises 26 p-type legs by embroidery of dyed silk fibers onto a piece of felted wool fabric (Ryan et al. 2017).

- **Inorganic TE fibers**

Conventional inorganic TE materials are rigid and brittle so that they are hard to be directly manufactured into flexible and freestanding fibers. Together with the insoluble feature, physical depositing methods such as thermal evaporation and magnetron sputtering were used for coating inorganic TE materials onto flexible fibers at first. In 2008, Yadav et al. prepared TE fiber by coating Ni and Ag layers onto flexible silica fibers via thermal evaporation and demonstrated power generation performance of the fiber-based TE generator (Yadav et al. 2008). Adjacent stripes of nickel and silver are deposited on one side of a silica fiber of diameter 710 μm by thermal evaporation under a vacuum of 5×10^{-7} Torr, as shown in Fig. 6a, b. First, a silver layer of thickness 120 nm is deposited through a mask; the mask is then moved
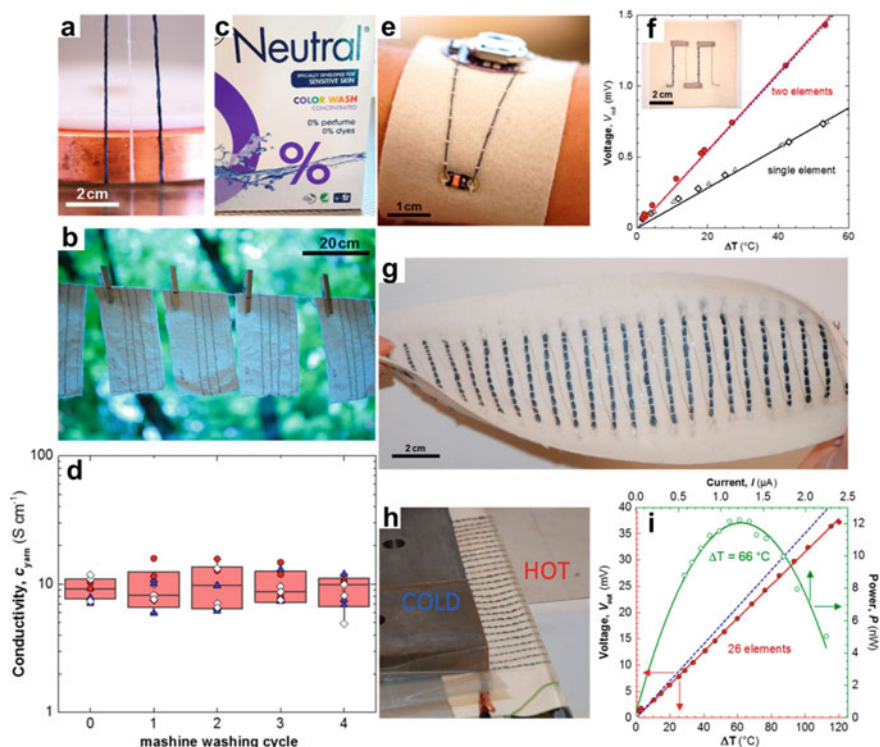
Fig. 5 **a** Neat and PEDOT:PSS dyed silk fibers submerged in distilled water; **b** PEDOT:PSS dyed silk fibers were sewn onto cotton fabrics and washed in a household Electrolux washing machine; **c** using Neutral COLOR WASH detergent; **d** electrical conductivity of PEDOT:PSS dyed silk fibers as a function of washing cycle (MeOH($\diamond$), EG (blue triangle), DMSO (red circle)); **e** Image of an LED connected with PEDOT:PSS dyed silk fibers to a battery (embroidered on felted wool fabric); **f** in-plane textile TE device with two ~5 cm long p-type legs of PEDOT:PSS dyed silk fibers (10 fibers per leg) connected with silver wire (inset) and output voltage as a function of applied temperature gradient (single element (black line), two elements (red line), calculated output (dotted line)); **g** in-plane textile TE device with 26 p-type legs prepared in a similar way as the two leg module, and **h** the device in use, suspended between a hot and cold temperature reservoir; **i** electrical measurements of the 26 leg module, showing output voltage a function of temperature gradient (all elements (red line), calculated (dotted line) $V_{out}/\Delta T$; see (**f**)) and power output as a function of measured current. Reproduced with permission. (Ryan et al. 2017) Copyright 2017, American Chemical Society

to cover the deposited silver, and a nickel layer of thickness 120 nm is deposited. The junctions are formed by a 0.5 mm overlap between the two metals. To test the thermoelectric properties of the fiber, they heated alternate junctions, resulting in a temperature gradient that mimics the heating profile of the fiber inside a woven pattern which has a temperature gradient normal to the surface. As shown in Fig. 6c, they used electrically insulated posts with heating wire wrapped around them as heat
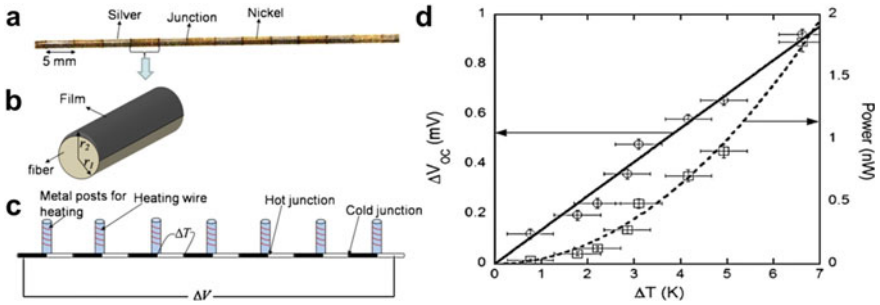
Fig. 6 **a** Picture of striped thin film TE fiber made with thermal evaporation of nickel and silver. **b** Illustration of fiber with thin film deposited on one side. **c** Schematic of experimental setup for applying a temperature gradient and measuring the induced open circuit voltage. **d** Net thermal voltage and maximum power output as a function of temperature applied for 7 couples. Reproduced with permission. (Yadav et al. 2008) Copyright 2007, Elsevier

sources, bringing alternate fiber junctions in contact with them. The unheated junctions were exposed to ambient (22 °C) and lose heat due to convection. Temperature differences between neighboring junctions are measured using micro thermocouples. Open circuit voltage versus temperature was measured, as well as the induced voltage across a matched load resistor. An open circuit voltage of 19.6 μV/K per thermocouple junction was measured for Ni-Ag fiber, and a maximum power of 2 nW for 7 couples at $\Delta T = 6.6$ K was measured (Fig. 6d).

Wang and his co-workers (Ren et al. 2016) explored the feasibility of a powder-processing-based method in the fabrication of inorganic Bi_2Te_3 TE fibers with large length-to-area ratio as shown in Fig. 7a, b. Powders were milled from Bi_2Te_3-based bulk materials and then mixed with a thermoplastic resin dissolved in an organic solvent. Through an extrusion process, flexible, continuous fibers with sub-millimeter diameters were formed. The polymer phase was then removed by sintering. Electrical resistivity of the sintered TE fibers was strongly affected by the sintering temperature such that increasing the sintering temperature led to decreased resistivity, which might be related to the residual porosity and grain boundary contamination. Electrical resistivity of the sintered fibers was as low as 14.1 mΩ·cm for p-type fibers sintered at 590 °C and 153 mΩ·cm for n-type fibers sintered at 580 °C, however, which were much higher than the corresponding bulk materials. The Seebeck coefficient of the fibers, on the other hand, exhibited comparable values to the bulk materials, implying that the Seebeck coefficient was not significantly affected by the sintering. The Seebeck coefficient is 179 μV/K and -207 μV/K for p-type $Bi_{0.5}Sb_{1.5}Te_3$ and n-type $Bi_2Te_{2.7}Se_{0.3}$ fiber, resulting the power factor of 1.7 μW/cmK^2 and 0.3 μW/cmK^2 for p-type fiber and for n-type fiber, respectively. Figure 7c is a picture of a prototype miniature uni-couple fabricated from the sintered fibers. High output power could be achieved by connecting multiple uni-couples either in series (with higher output voltage) or in parallel (with higher output current). For example, Fig. 7d shows the performance of two uni-couples connected in series, where the maximum output power was increased to 18 nW and the corresponding output voltage was
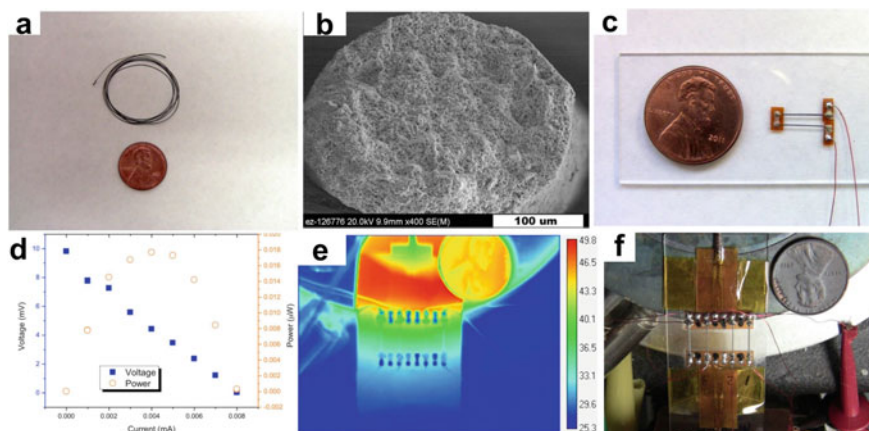
Fig. 7 **a** An as-extruded fiber, **b** the cross section of a p-type fiber sintered at 590 °C in vacuum for 4 h. **c** Prototype miniature uni-couple fabricated from sintered fibers and **d** I–V curve and power output of a module consisting of two uni-couples connected in series. **e** Infrared image of a prototype module consisting of two uni-couples showing the temperature distribution in the module at equilibrium, and **f** its corresponding digital picture. Reproduced with permission. (Ren et al. 2016) Copyright 2015, Springer Nature

increased to 4.8 mV. Figure 7e is the infrared image of this two uni-couple module showing the temperature distribution at thermal equilibrium; the hot size and cold side temperatures were approximately 42 and 30 °C, respectively. The corresponding picture of this module is shown in Fig. 7f. Prototype modules consisting of up to 4 uni-couples (8 fiber elements) were constructed and the power output and the voltage (or the current) were quadrupled compared to single uni-couples. Due to the large electrical resistivity, these prototype uni-couples and modules fabricated from such fibers showed poor performance in terms of power output. Therefore, further studies are highly desirable to seek improved sintering conditions to optimize the fiber compositions and to reduce their porosity.

Graphene fibers have been extensive researched in sensing devices, energy harvesters and supercapacitor on account of its superior mechanical properties and high electrical conductivity. In contrast with traditional wet- or dry-spinning techniques, self-assembly in tube module is a more accessible method to prepare graphene fibers (Xu et al. 2020). Furthermore, the semiconductor behavior of graphene is easily to be converted from p-type to n-type via doping of electron donating molecules, providing us an inspiration to prepare an integral p-n connected graphene TE fiber. Lin et al. (2019) obtained an integral p-n connected all-graphene fiber without any additional conductive adhesive and assembled a wearable fiber-based TE energy-harvesting device. As shown in Fig. 8, graphene oxide (GO) dispersion was prepared by oxidation of natural graphite powder via modified Hummers' method. Homogeneously mixed GO and ascorbic acid (AA) hybrid solution was sealed in polytetrafluoroethylene (PTFE) tube. The GO fiber was kept at 80 °C for 2 h. The GO fiber was further reduced with $N_2H_4 \cdot H_2O$ to achieve a higher TE performance, which
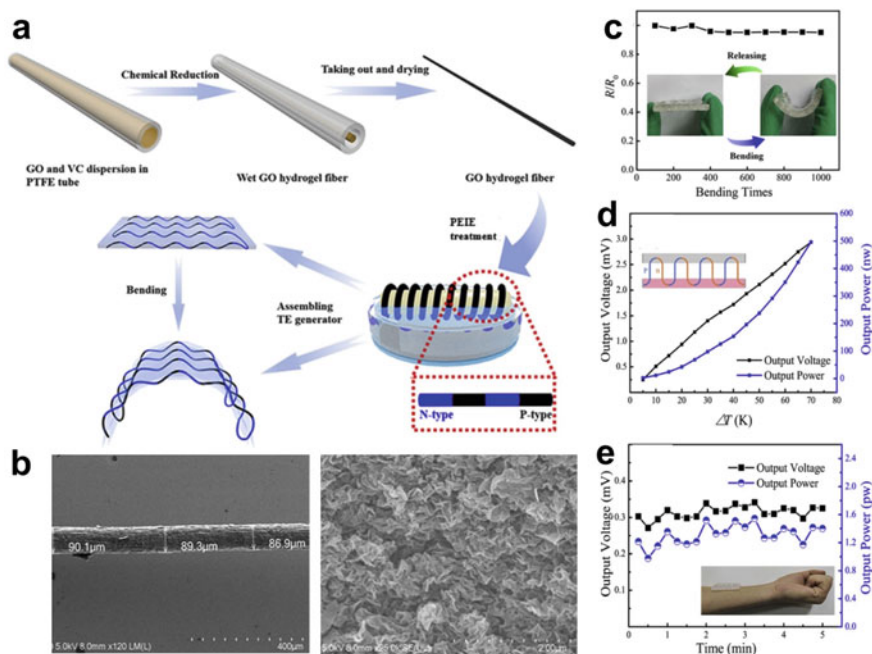
Fig. 8 **a** Schematic illustration of the fabrication process of an integral p-n connected all-graphene fiber. **b** SEM images of GO fibers and its surface morphology. **c** Digital photographs of TE generators. **d** The output voltage and output power of p-n connected TE fibers at various temperature differences ranging from 5 to 70 K. **e** The stability with time for output performance of TE generators. Reproduced with permission. (Lin et al. 2019) Copyright 2019, Elsevier

was noted as p-GO fiber. Then, to obtain an integral p-n connected all-graphene fiber, as-prepared GO fiber was rolled onto a plastic rod and partially immersed into polyethyleneimine ethoxylated (PEIE) solution, which was noted as p-n-GO fiber. Finally, the integral p-n connected all-graphene fiber was integrated into poly-dimethylsiloxane (PDMS) to achieve a flexible fiber-based TE device. Young's modulus of GO fiber was calculated as 18.4 GPa. After treated with $N_2H_4 \cdot H_2O$, Young's modulus increased about 40% to 25.8 GPa for p-GO fiber, which might be ascribed to the reductant-induced enhancement of π-π stacking interactions between graphene sheets. For n-GO fiber, Young's modulus decreased to 12.8 GPa compared to that of p-GO fiber. They assembled a wearable TE energy-harvesting device via integrating a p-n-GO fiber consisting of 20 pairs p-n legs into flexible PDMS substrate (Fig. 8c). Mechanical reliability is an important indicator for wearable device. They tested the electrical resistance variation of this fiber-based device for about 1000 times of bending-releasing circle. The initial electrical resistance was measured as about 75 kΩ and the electrical resistance maintained almost the same with about less than 5% variation, indicating a good mechanical reliability of this device (Fig. 8c). The output voltage and power of this fiber-based device consisting of 4 pairs of p-n

legs were calculated under the temperature gradient ranging from 0 to 70 K. As shown in Fig. 8d, one can see that the maximal output voltage and output power were calculated 0.75 mV and 124.1 nW per p-n leg under 70 K temperature difference. Furthermore, Fig. 8e recorded a practical measurement results of the output voltage and power for several minutes at temperature difference between human body and air temperature ($\Delta T = 10 \pm 0.5$ K), indicating a stable TE energy-harvesting performance.

Most CNT-based TE generators have been fabricated via alternative stacking/or printing of p- and n-type CNT films/or inks with metal deposition as an electrode between p- and n-type units. However, in the case of highly electrically conductive CNT, the contact resistance between metal electrode and CNT is higher than the resistance of metal or CNT itself, thus decreasing the output power density of flexible TE generators. Choi et al. (2017) reported a robust CNT fiber with excellent electrical conductivity of 3147 S cm^{-1} which is due to increased longitudinal carrier mobility derived from highly aligned structure. On the basis of highly conductive CNT fiber, they fabricated an all-carbon TE generator with superior TE performance. Figure 9a shows a schematic of flexible TE generator based on CNT fiber without metal electrodes. The synthesized CNT fiber was wound onto a flexible supporting unit, and alternatively doped into n- and p-types using polyethylenimine (PEI) and FeCl$_3$ solutions, respectively, with undoped material between the two doped regions. The CNT fiber between the doped regions was used as electrodes to minimize the circuit resistance because it has excellent electrical conductivity. The CNT fiber used in TEG fabrication was continuously produced by direct spinning after synthesis. Thousands of individual double-walled CNTs compose a CNT fiber of 30 μm in diameter as shown in the scanning electron microscopy (SEM) images in Fig. 9b. Highly integrated CNT fibers have a density of ~1.0 g/cm3 and high specific strength of ~1 GPa/(g·cm^{-3}). Furthermore, the CNT fiber has excellent specific electrical conductivity on the order of 103 S·cm^2/g, which is comparable to some metals (Fig. 1c). On the basis of mechanical strength and shape advantage of CNT fiber for modular fabrication, various types of flexible TE generators were prepared. A prototype flexible TE generator with 60 pairs of n- and p-doped CNT fiber shows a maximum power density of 10.85 and 697 μW/g at temperature differences (ΔT) of 5 and 40 K, respectively, which are the highest values among reported TE generators based on flexible materials (Fig. 9d–f). Furthermore, the flexible TE generator based on 240 pairs of n- and p-doped CNT fiber can successfully power a red LED using an energy-harvesting circuit at $\Delta T = 50$ K (Fig. 9g–i).

- **Organic/inorganic composite TE fibers**

As discussed in the previous sections, the TE properties of conducting polymers have been significantly improved; however, they are still much lower than those of inorganic thermoelectric materials. However, for flexible TE devices, the use of inorganic materials is in general hampered by their inherent rigidity. Overcoming
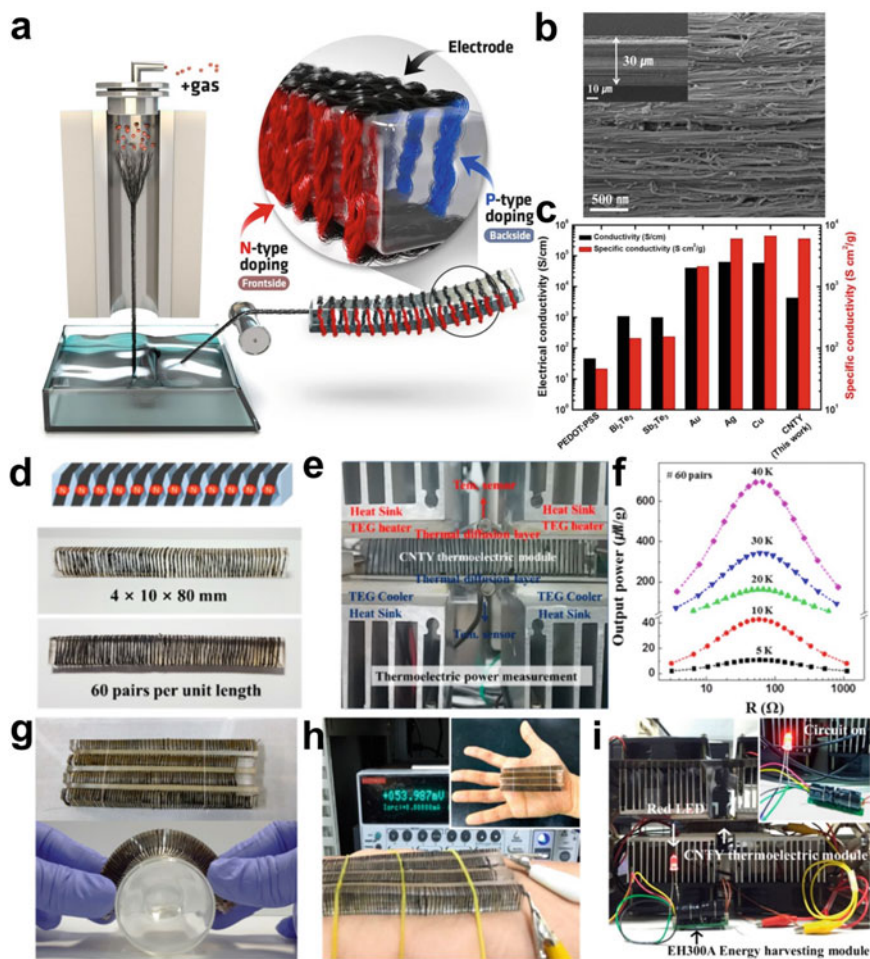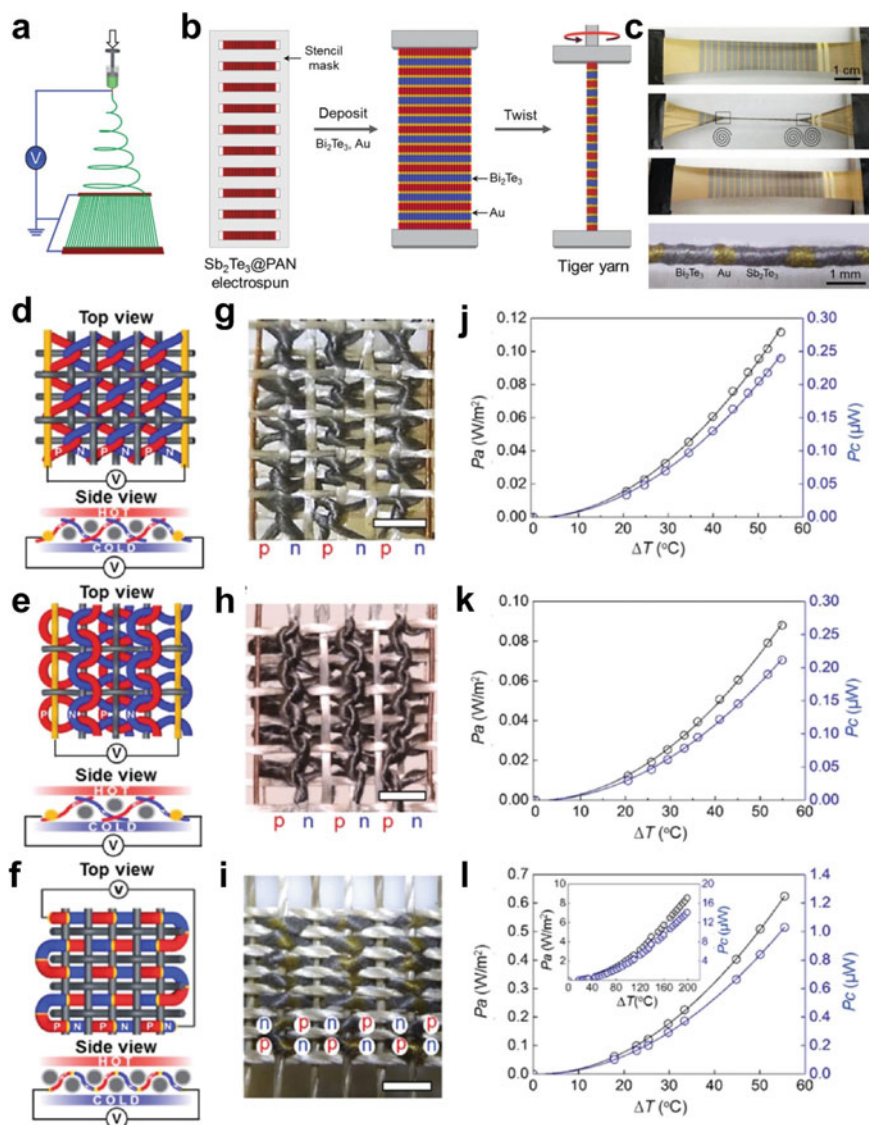
Fig. 9 **a** Schematic illustration of the flexible TE generator based on CNT fiber. **b** SEM image of the CNT fiber. **c** Electrical conductivity and specific conductivity of the CNT fiber and typical conducting materials. **d** Photograph of fiber-based TE generator with 60 PN pairs. **e** Photograph of power measurement system. **f** Output power density of fiber-based TE generator with 60 PN pairs as a function of load resistance. **g** Photographs showing the practical application of flexible fiber-based TE generator. **h** Output voltage of fiber-based TE generator obtained from the temperature difference between body heat and atmosphere. **i** Photograph showing a red LED powered using fiber-based TE generator at $\Delta T = 50$ K. Reproduced with permission. (Choi et al. 2017) Copyright 2017, American Chemical Society

this issue is to prepare organic/inorganic composite TE fibers. The most obvious manners are to deposit inorganic materials onto a flexible organic fiber substrate, or embed inorganic materials into a flexible organic fiber substrate.

Lee and his co-workers proposed the fabrication of flexible, woven, and knitted textiles based on electrospun organic polymer nanofiber cores that are coated with inorganic n- and p-type semiconductor sheaths (Bi_2Te_3 and Sb_2Te_3, respectively) and twisted into flexible TE fibers (Lee et al. 2016). Separate n-type and p-type fibers were prepared by depositing Bi_2Te_3 and Sb_2Te_3, respectively. Highly aligned sheets of polyacrylonitrile (PAN) nanofibers, with average nanofiber diameter of $\approx$ 600 nm, were electrospun on two parallel wire collectors (Fig. 10a). A PAN solution in the syringe is extruded through the metal needle. A high voltage supply is connected to the spinning tip and to two counter electrodes, so that highly aligned PAN nanofiber sheets are collected. Tiger-type fibers were fabricated by first sputtering alternating strips of Sb_2Te_3 and Bi_2Te_3 (Fig. 10b) on both sides of the electrospun PAN nanofiber sheet using a stencil mask which produces sheath-core nanofiber structures containing $\approx$ 50% by volume of active material and then interconnecting these TE strips using narrow sputtered gold strips. The thicknesses of these coatings were 110 nm for the TE materials and 75 nm for the gold. The thereby coated nanofiber sheets were then twisted into yarns using an electric motor, typically using a twist density of $\approx$ 630 turns per meter, relative to the initial sheet length, followed by a thermal annealing at 200 °C to crystallize the semiconductors, resulting in a strong, flexible sheath-core TE fiber. Figure 10c demonstrates that the initial tiger structure is retained during twist insertion and subsequent complete fiber untwist. The power output of 3D fiber-based TE generators assembled in different fabric structures was also investigated. Figure 10d–i displays the schematic illustrations and photographs of zigzag-stitch, garter-stitch, and plain-weave TE generators using p-type Sb_2Te_3 fibers and n-type Bi_2Te_3 fibers. At temperature difference of 55 K, the power output per area and per couple were 0.11 W m^{-2} and 0.24 μW for the zigzag-stitch TE generator (Fig. 10j), and 0.09 W m^{-2} and 0.21 μW for the garter-stitch TE generator (Fig. 10k), respectively, while the plain-weave TE generator (Fig. 10l) presented the highest power output per area of 0.62 W m^{-2} and 1.01 μW per couple, respectively. Besides, the power output was proportional to ΔT^2. When the temperature difference increased to 200 K, the generated power greatly increased to 8.56 W m^{-2} and 14.1 μW per couple, respectively.

Inversely, Sun et al. (2020) presented and developed a π-type inorganic CNT fiber-based TE module using organic PEDOT:PSS and oleamine doping combined with electrospray technology. Figure 11a schematically exhibited the fabrication process of TE modules. First, CNT fiber was p-hybridized by dipping into a commercial PEDOT:PSS solution. Subsequently, n-type CNT fiber was achieved in an equal interval using polypropylene mask by oleamine doping combined with electrospray technology. Therefore, a TE fiber with alternatively doped n- or p- segment at the distance of (L-4 mm)/2 was formed, where L (mm) is the length of p-n repeat unit of the fiber. The 2 mm long undoped section is electrically conducting and treated as
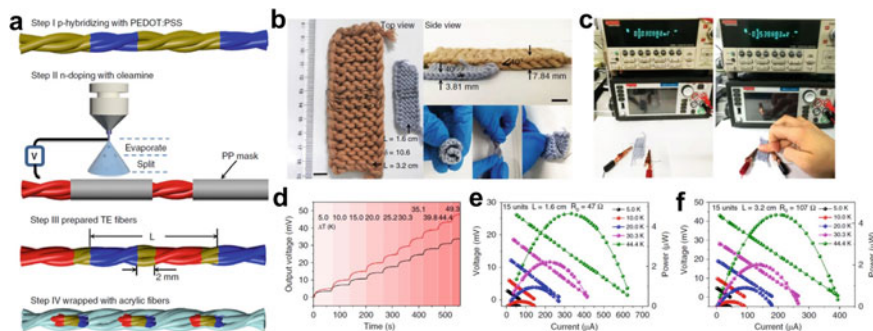
Fig. 10 **a** Illustration of the electrospinning process used to make PAN nanofiber sheets for conversion into a yarn. **b** Illustration of the stencil mask-based method used to provide alternating p-Au-n segments for tiger fibers by sequentially sputtering Sb_2Te_3-gold-Bi_2Te_3 on both sides of a PAN nanofiber sheet. **c** Illustration of the twist spinning process used to convert the nanofiber sheet into a tiger fiber. **d**–**f** Schematic illustrations and **g**–**i** corresponding photographs of the fabricated zigzag-stitch, garter-stitch, and plain-weave fiber-based TE generators. The scale bars are 2 mm. **j**–**l** The power output per textile area (Pa) and per TE couple (Pc) of the fabricated zigzag-stitch, garter-stitch, and plain-weave fiber-based TE generators as a function of temperature difference. Reproduced with permission. (Lee et al. 2016) Copyright 2016, Wiley-VCH

Fig. 11 **a** p-Hybridized CNT and n-Doped CNT TE fibers fabricated by an electrospray technique wrapped with acrylic fibers. **b** Photograph of TE generator composed of 15 units (3 × 5) with different TE repeat length L. Scale bars, 1 cm. **c** The output voltage display of TE generator (15 units) with repeat length of 16 mm before and after fingertip touching. **d** The output voltage contrast of the two TE generators at various steady temperature differences given by Peltier elements. **e**, **f** Power output of the TE generators with L of 16 mm/32 mm at various steady temperature differences. R_0 is the internal resistance of TE generators. Reproduced with permission. (Sun et al. 2020) Copyright 2020, Springer Nature

an electrical interconnection between the two doped sections. Furthermore, to avoid a short circuit, the doped CNT fiber was wrapped with acrylic fibers using a cover spun technique, except the electrode segment, which was exposed to maximize the thermal contact between the TE generator and the human body.

A high tightness δ of 10.6 is given and the TE repeat length L of TE generator with the same amount of units was adjusted from 32 to 16 mm to optimize power density. A dramatically decreased occupied area can be seen in Fig. 11b. Besides, the thickness of the TE generator reduced from 7.8 to 3.8 mm, but the ~40° standing angles of TE legs were maintained. Figure 11b also shows the ability of the prepared TEG to adapt to various loading conditions, for example, bending, twisting, and folding. Furthermore, a 3.5 mV voltage can be immediately detected when human fingertip touches the small TE generator as shown in Fig. 11c. The output voltage at various steady temperature differences are displayed in Fig. 11d. When a through thickness temperature difference is applied, an obvious Seebeck voltage is immediately created. After reducing the repeat length to 16 mm, the voltage decreases by ~26%, in accordance with the positive dependence of temperature difference ΔT across TE legs on repeat length L. Conversely, the power increases after reducing the repeat length to 16 mm as shown in Fig. 11e, f. Using 44.4 K temperature difference, the power enhances from 4.40 to 4.64 μW, accompanying an short circuit current increasing from ~450 to ~700 μA. A 4-fold rise in power density is obtained after reducing the repeat length from 32 to 16 mm. Giving 44.4 K temperature difference, the power density increases from 14 μWm^{-2} with $L = 32$ mm to 69 μWm^{-2} with $L = 16$ mm, which is the highest output reported for a flexible organic TE generator.

Recently, thermal drawing technique was developed to produce inorganic TE fibers such as $Bi_{0.5}Sb_{1.5}Te_3$, Bi_2Se_3, $(Te_{85}Se_{15})_{45}As_{30}Cu_{25}$, In_4Se_3, and Bi_2Te_3 fibers
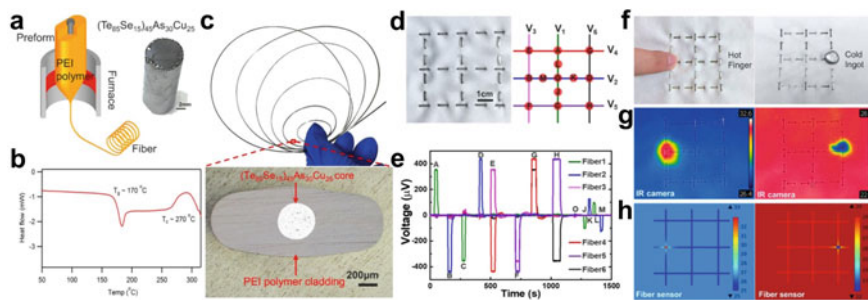
Fig. 12 **a** Schematic diagram of the drawing process of a TE fiber from the semiconducting glass rod and PEI polymer. **b** Glass transition temperature (T_g) and crystallization temperature (T_x) of the semiconducting glass measured by differential scanning calorimeter (DSC). **c** Single TE fiber with good flexibility and the optical microscope image of fiber cross section. **d** Photograph of the fabricated 3×3 TE fiber array embedded into a flexible fabric and the marked points for finger touching. **e** Corresponding output voltages of the TE fiber array when touching the marked points. **f** Finger heating (33 °C) and ingot cooling (22 °C) on the TE fiber array. Corresponding **g** thermal images recorded by IR camera and **h** reconstructed thermal maps using the data of TE fiber. Reproduced with permission. (Zhang et al. 2019) Copyright 2019, American Chemical Society

(Loke et al. 2020; Zhang et al. 2017, 2019). The process required a cladding material with glass transition temperature slightly higher than the melting point of TE materials. The TE fibers fabricated by this method usually had high TE properties but general mechanical flexibility. For example, Zhang et al. (2019) prepared flexible $(Te_{85}Se_{15})_{45}As_{30}Cu_{25}$ fiber was prepared by thermal drawing. Figure 1a schematically shows the preform-based fabrication of TE fibers. A semiconducting glass rod of $(Te_{85}Se_{15})_{45}As_{30}Cu_{25}$ shown in the inset of Fig. 12a is first synthesized by a standard sealed-ampoule technique (Lucas et al. 2013), and this semiconducting glass offers two superior properties in constructing flexible thermal sensors. One is that its Seebeck coefficient is large enough to ensure the sensitivity of thermal sensing. The other is that its glass transition temperature (T_g) is 170 °C and the crystallization temperature (T_c) is 270 °C, as measured in Fig. 12b, offering a wide glass stability range of 100 °C, which makes it particularly suitable for the thermal fiber drawing process with the polymer matrix. Then, a hollow rectangle-shaped PEI polymer tube with a softening temperature of 217 °C is used to support and confine $(Te_{85}Se_{15})_{45}As_{30}Cu_{25}$, while providing excellent mechanical properties. The synthesized semiconducting glass is reshaped and filled in the hollow PEI block, and then the entire assembly is thermally sealed in a vacuum oven to form an all-solid macroscopic preform. The preform is further loaded in a fiber draw tower with a narrow heating zone and thermally drawn at the temperature of 250 °C, where the viscosity of the PEI cladding is much larger than that of the TE glass core, thus supporting the whole structure and yielding hundreds of meters of TE fibers. Figure 12c shows the photograph of the resulting TE fiber and its optical microscope image of the cross section. Owing to the presence of polymer cladding, the resulting fiber exhibits high mechanical flexibility to be easily bent, coiled, and woven. The continuous

semiconducting glass core and polymer cladding are well maintained in a round and rectangular shape, respectively, and the interfaces between the core and cladding are clearly defined. The required TE fiber dimension can be precisely controlled via adjusting the feeding speed of the preform and the drawing speed of the fiber.

The fiber displayed not only high TE power factor but also excellent thermal sensing performance, as illustrated in Fig. 12d–h. When a temperature difference was applied between the two fiber ends, thermoelectric voltage was generated because of the whole diffusion. The single TE fiber-based thermal sensor showed temperature resolution higher than 0.05 °C. Additionally, it was capable of localizing the position of thermal source, because the output voltages were different when touching different positions along the fiber. More importantly, the TE fiber showed good mechanical flexibility. The bending radius was only ~2.5 mm even for the fiber with thickness of 0.6 mm. Nonetheless, it was hard to simultaneously detecting the temperature and position of thermal source in the single TE fiber-based thermal sensor. The authors further assembled a 3×3 TE fiber array and embedded it into a flexible fabric (Fig. 12d). Figure 12e recorded the output voltages of the TE fiber array when finger touching the marked points. The distinguishable voltage signals enabled the simultaneous detection of the temperature and position of thermal source. Figure 12f gave two examples for temperature and position identification, one is finger heating (33 °C) and another is ingot cooling (22 °C). The corresponding thermal images recorded by IR camera and reconstructed thermal maps using the data of TE fiber array were shown in Fig. 12g, h, respectively.

Similarly, Zhang et al. (2017) prepared flexible p-type $Bi_{0.5}Sb_{1.5}Te_3$ and n-type Bi_2Se_3 fibers by thermal drawing and assembled them into textile to construct TE generator (Fig. 13a-c). The prepared p-type $Bi_{0.5}Sb_{1.5}Te_3$ fiber exhibits power factor of 3520 $\mu Wm^{-1}K^{-2}$ and n-type Bi_2Se_3 fiber with power factor of 650 $\mu Wm^{-1}K^{-2}$, respectively. Due to the p-type $Bi_{0.5}Sb_{1.5}Te_3$ with the melting point of 873 K and n-type Bi_2Se_3 with the melting point of 983 K as the TE fiber cores, so the borosilicate glass tube with the glass transition temperature of 1100 K is the best choice for the cladding material, as schematically shown in Fig. 13a. To prevent oxidation of the inserted TE rod during the drawing process, the empty space inside the glass tube is filled up with borosilicate glass rods, and the entire assembly is sealed from both ends under vacuum. The preform is then loaded in a fiber draw tower, fed into the furnace, and thermally drawn at the temperature of 1323 K, where the viscosity of the glass cladding is large enough to offer a structural support to the liquid TE cores, thus yielding hundreds of meters of continuous TE fibers. A polymer coating layer with the thickness of 50–150 μm depending on the resulting fiber diameter is then applied to the fiber outer surface for further mechanical protection. Figure 13b shows the photograph of a single bent TE fiber with the length of one meter and its SEM image of cross section. The fiber possesses good circularity and a clean interface between the concentric TE core and the glass cladding. The diameters of TE core and glass cladding are 33 μm and 400 μm, respectively, which has nearly the same diameter ratio of the TE rod (0.8 mm) and glass tube (10 mm) in the original preform, proving that such a thermal drawing is a proportional size-reduction process.
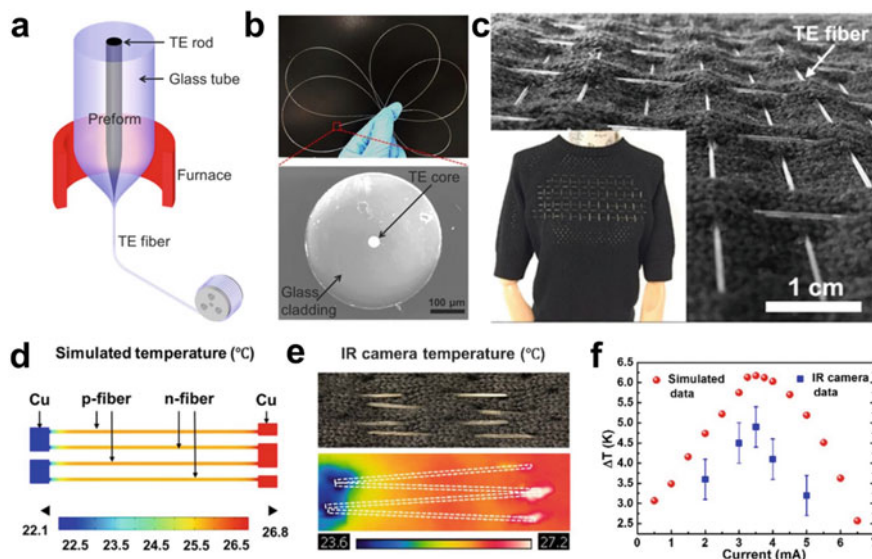
Fig. 13 **a** Schematic diagram of the thermal drawing process. **b** Single TE fiber with a length of one meter showing a good flexibility and its cross-sectional SEM image. **c** TE fibers are woven into a large-area fabric to construct a wearable TE device. **d** Simulated temperature profile of TE cooling with two pairs of p-n TE fibers at an input current of 2 mA by finite element modeling. **e** Corresponding experimental temperature profile recorded by IR camera. **f** Simulated and experimental temperature differences as a function of input current. Reproduced with permission. (Zhang et al. 2017) Copyright 2017, Elsevier

To engage the TE fibers for flexible and wearable electronics on large areas, they constructed the TE fibers into a two-dimensional fabric (Fig. 13c). These fibers possess many extraordinary characteristics such as thin, lightweight, and flexible to deform under small external force, so the TE fiber woven fabrics can be sufficiently sparse to maintain breathability of the covered areas, which is a critical requirement of long-term comfort around curvilinear human skins, and can be used as a TE cooler to cool the human body via a low impressed current. The cooling performance of TEG with two pairs of TE fibers was evaluated by finite element modeling and experimental characterizations. In Fig. 13d, the simulated temperature reduction was 22.1 °C with the temperature difference of 4.7 °C when the hot side was fixed at 26.8 °C under an input current of 2 mA. The measured temperature reduction was 23.6 °C with the temperature difference of 3.6 °C recorded by IR camera (Fig. 13e). The difference between simulation and test results might be induced by the measurement accuracy of IR camera as well as the unoptimized condition of TE generator. Figure 13f displays both the simulated and experimental temperature differences as a function of input current. Maximum temperature reduction of ~5 °C was obtained when the input current was 3.5 mA.

3   Conclusion

In this chapter, an overview and review of state-of-the-art flexible TE fiber materials and devices were presented with respect to the materials mechanism, fabrication methods, device structures, and application performance. Organic TE fibers such as PEDOT;PSS are flexible with high electrical conductivity and processed at low or room temperature via solution routes (wet-spinning, electrospinning, and dyeing process). Inorganic TE fibers fabricated by coating, extruding, and printing approaches have relatively high performance, but the high cost, limited flexibility, and complicated fabrication limit their development. However, organic/inorganic composite TE fibers fabricated by surface modification (physical/chemical deposition) or embedding approaches (thermal drawing) simultaneously have inorganic semiconductor-like high TE performance and organic material-like mechanical flexibility, which shows great potentials to power and refrigerate wearable electronic devices.

Although flexible TE fibers exhibit enormous application potential, TE fiber materials and devices in the early stage of development. The studies on TE generators made up of TE fibers are very few and the device performance is much lower than that of bulk TE materials based TE generators. To achieve more advancements of TE fiber, the performance and stability of the fiber should be firstly improved significantly. Then, the effects such as the device structure resulted from different textile techniques and the size of TE legs on the device performance of fiber-based TE generators should be further explored. Moreover, instruments to measure the thermal conductivity, Seebeck coefficient, and electrical conductivity of the TE fiber are homemade in most cases and lack of standardized measurement at present. Finally, current fabrication methods are mostly limited to the laboratory and are difficult to realize in mass production, which should be further explored. In a word, TE fibers have presented promising applications in smart wearable electronics, and there is huge room for the development and practical applications of fiber-based TE generators.

References

C. Chang et al., Science **360**, 778 (2018)
Y. Chen, Y. Zhao, Z. Liang, Energy Environ. Sci. **8**, 401 (2015)
J. Choi et al., ACS Nano **11**, 7608 (2017)
G.B. Delkumburewatte, T. Dias, J. Textile Inst. **103**, 483 (2012)
M.S. Dresselhaus, G. Chen, M.Y. Tang, R.G. Yang, H. Lee, D.Z. Wang, Z.F. Ren, J.-P. Fleurial, P. Gogna, Adv. Mater. **19**, 1043 (2007)
Y. Du, K.F. Cai, S. Chen, P. Cizek, T. Lin, ACS Appl. Mater. Interfaces. **6**, 5735 (2014)
Y. Du, K.F. Cai, S.Z. Shen, R. Donelsonand, J.Y. Xu, H.X. Wang, T. Lin, RSC Adv. **7**, 43737 (2017)
Y. Du, J. Xu, B. Paul, P. Eklund, Appl. Mater. Today **12**, 366 (2018)
L. Wang, K. Zhang, Energy Environ. Mater. 0, 1 (2019)
R. Fitriani, B.D. Ovik, M.C. Long, M. Barma, M.F.M. Riaz, S.M. Sabri, Said, R. Saidur, Renew. Sustain. Energy Rev. **64**, 635 (2016)

C. Gao, G. Chen, Small **14**, 1703453 (2018)

J. Gao, C. Liu, L. Miao, X. Wang, Y. Peng, Y. Chen, J. Electronic Mater. **46**, 3049 (2017)

T.C. Harman, P.J. Taylor, M.P. Walsh, B.E. LaForge, Science **297**, 2229 (2002)

W. He, G. Zhang, X. Zhang, J. Ji, G. Li, X. Zhao, Appl. Energy **143**, 1 (2015)

Q. Jin et al., Nature Mater. **18**, 62 (2019)

G.H. Kim, L. Shao, K. Zhang, K.P. Pipe, Nature Mater. **12**, 719 (2013)

N. Kim, S. Kee, S.H. Lee, B.H. Lee, Y.H. Kahng, Y.-R. Jo, B.-J. Kim, K. Lee, Adv. Mater. **26**, 2268 (2014)

S.J. Kim, H.E. Lee, H. Choi, Y. Kim, J.H. We, J.S. Shin, K.J. Lee, B.J. Cho, ACS Nano **10**, 10851 (2016)

Y. Lan, A.J. Minnich, G. Chen, Z. Ren, Adv. Functional Mater. **20**, 357 (2010)

J. Lee, B. Llerena Zambrano, J. Woo, K. Yoon, T. Lee, Adv. Mater. 32, 1902532 (2020)

J.A. Lee et al., Adv. Mater. **28**, 5038 (2016)

J.-F. Li, W.-S. Liu, L.-D. Zhao, M. Zhou, NPG Asia Mater. **2**, 152 (2010)

Y. Lin, J. Liu, X. Wang, J. Xu, P. Liu, G. Nie, C. Liu, F. Jiang, Compos. Commun. **16**, 79 (2019)

J. Liu et al., ACS Appl. Mater. Interfaces. **10**, 44033 (2018)

G. Loke, W. Yan, T. Khudiyev, G. Noel, Y. Fink, Adv. Mater. **32**, 1904911 (2020)

P. Lucas et al., J. Mater. Chem. A **1**, 8917 (2013)

C. Müller, M. Hamedi, R. Karlsson, R. Jansson, R. Marcilla, M. Hedhammar, O. Inganäs, Adv. Mater. **23**, 898 (2011)

H. Park, S.H. Lee, F.S. Kim, H.H. Choi, I.W. Cheong, J.H. Kim, J. Mater. Chem. A **2**, 6532 (2014)

S.H. Park et al., Nature Commun. **7**, 13403 (2016)

B. Paul, J. Lu, P. Eklund, ACS Appl. Mater. Interfaces. **9**, 25308 (2017)

F. Ren, P. Menchhofer, J. Kiggans, H. Wang, J. Electronic Mater. **45**, 1412 (2016)

J.D. Ryan, D.A. Mengistie, R. Gabrielsson, A. Lund, C. Müller, ACS Appl. Mater. Interfaces. **9**, 9045 (2017)

G.J. Snyder, E.S. Toberer, Nature Mater. **7**, 105 (2008)

T. Sun, B. Zhou, Q. Zheng, L. Wang, W. Jiang, G.J. Snyder, Nature Commun. **11**, 572 (2020)

R. Venkatasubramanian, E. Siivola, T. Colpitts, B. O'Quinn, Nature **413**, 597 (2001)

C. Wan et al., Nature Mater. **14**, 622 (2015)

Y. Wang, L. Yang, X.-L. Shi, X. Shi, L. Chen, M.S. Dargusch, J. Zou, Z.-G. Chen, Adv. Mater. **31**, 1807916 (2019)

L. Wang, X. Fu, J. He, X. Shi, T. Chen, P. Chen, B. Wang, H. Peng, Adv. Mater. **32**, 1901971 (2020)

T. Xu, Z. Zhang, L. Qu, Adv. Mater. **32**, 1901979 (2020)

A. Yadav, K.P. Pipe, M. Shtein, J. Power Sources **175**, 909 (2008)

C. Yang et al., Nature Commun. **8**, 16076 (2017)

L. Yang, Z.-G. Chen, M.S. Dargusch, J. Zou, Adv. Energy Mater. **8**, 1701797 (2018)

R. Yue, J. Xu, Synth. Met. **162**, 912 (2012)

T. Zhang, K. Li, J. Zhang, M. Chen, Z. Wang, S. Ma, N. Zhang, L. Wei, Nano Energy **41**, 35 (2017)

L. Zhang, S. Lin, T. Hua, B. Huang, S. Liu, X. Tao, Adv. Energy Mater. **8**, 1700524 (2018)

J. Zhang, S. Seyedin, S. Qin, P.A. Lynch, Z. Wang, W. Yang, X. Wang, J.M. Razal, J. Mater. Chem. A **7**, 6401 (2019a)

T. Zhang et al., ACS Appl. Mater. Interfaces. **11**, 2441 (2019b)

L.-D. Zhao, S.-H. Lo, Y. Zhang, H. Sun, G. Tan, C. Uher, C. Wolverton, V.P. Dravid, M.G. Kanatzidis, Nature **508**, 373 (2014)

Y.-H. Zhu, X.-Y. Yang, T. Liu, X.-B. Zhang, Adv. Mater. **32**, 1901961 (2020)